



## OPEN Enhancing wound healing with synergistic dual-drug electrospun roflumilast and L-arginine loaded PLA/PVA nanofibers through fabrication, optimization, and *in vivo* assessment

Samar A. Salim<sup>1</sup>✉, Abdullah M. M. Elbadry<sup>2</sup>, Esraa B. Abdelazim<sup>3</sup>, Tasneem Abed<sup>3</sup>, Marwa Mosaad Shakweer<sup>4,5</sup>, Noura G. Eissa<sup>3,6</sup>, Elbadawy A. Kamoun<sup>7,8</sup>✉ & Mahmoud Elsabahy<sup>3,9</sup>✉

Current trends in improved wound management emphasize the development of dual-drug-loaded electrospun nanofibrous scaffolds. Herein, electrospun dual-drug loaded PLA/PVA nanofibrous scaffolds, incorporating roflumilast, a selective phosphodiesterase-4 inhibitor with anti-inflammatory activity, and L-arginine, a precursor to nitric oxide with stimulating activity towards wound healing and tissue regeneration, were developed. A dual-spinneret electrospinning process enabled the co-loading of drugs in PLA and PVA phases. Scaffolds were characterized by SEM, FTIR, and XRD, showing consistent fiber morphology, and amorphous drug formation. FTIR analysis was performed to confirm drug-polymer compatibility and successful incorporation of roflumilast and L-arginine within the PLA/PVA nanofibrous matrix. Swelling ratio analysis indicated controlled hydration behavior regarding polymer-drug composition, and dual-drug-loaded fibers exhibited maximum initial swelling (610%) and stabilization at ~240%. *In vivo* rat excision wound healing model showed that the dual-drug loaded nanofibers demonstrated enhanced wound healing with ~99.8% healing on day 14, which was significantly better, compared to nanofibers incorporating a single drug and control groups. Moreover, histological studies revealed the absence of residual granulation tissue and enhanced re-epithelialization in the dual-drug treated group. These results indicate that roflumilast and L-arginine co-loaded PLA/PVA nanofibers exhibit wound-healing and regenerative properties, offering a promising therapeutic platform for enhanced wound repair.

**Keywords** Electrospinning, Dual-drug, Nanofibers, Roflumilast, L-arginine, Wound healing, PLA, Drug delivery

The skin is the largest organ in the body, essential for various functions including excretion, vitamin D synthesis, protection against pathogens, hydration maintenance, and temperature regulation. Severe dermal injuries

<sup>1</sup>Nanotechnology Research Center (NTRC), The British University in Egypt (BUE), El-Sherouk City, Cairo 11837, Egypt. <sup>2</sup>Department of Pharmaceutics and Industrial Pharmacy, Faculty of Pharmacy, Galala University, New Galala 43713, Egypt. <sup>3</sup>Badr University in Cairo Research Center, Badr University in Cairo, Badr City, Cairo 11829, Egypt. <sup>4</sup>Department of Pathology, Faculty of Medicine, Badr University in Cairo, Cairo 11829, Egypt. <sup>5</sup>Department of Pathology, Faculty of Medicine, Ain Shams University, Cairo, Egypt. <sup>6</sup>Department of Pharmaceutics, Faculty of Pharmacy, Zagazig University, Zagazig 44519, Egypt. <sup>7</sup>Department of Chemistry, College of Science, King Faisal University, Al-Ahsa 31982, Saudi Arabia. <sup>8</sup>Polymeric Materials Research Department, Advanced Technology and New Materials Research Institute (ATNMRI), City of Scientific Research and Technological Applications (SRTA-City), Alexandria 21934, Egypt. <sup>9</sup>Department of Pharmaceutics, Faculty of Pharmacy, Assiut University, Assiut 71526, Egypt. ✉email: samar.salim@bue.edu.eg; ekamoun@kfu.edu.sa; mahmoud.elsabahy@buc.edu.eg

may be life-threatening, and the wound healing process exhibits numerous remarkable cellular and molecular mechanisms. The repair process involves several interactions among cells, growth factors, and cytokines to facilitate lesion closure<sup>1,2</sup>. Various types of wound dressings are currently available, including films, hydrogels, and electrospun nanofibers (NFs). These dressings create a moist, regulated environment that facilitates cellular growth and migration, leading to accelerated wound healing<sup>3,4</sup>. However, the painful removal of films and the fact that they apply mainly to non-highly exuding wounds are considerable limitations<sup>5</sup>. Hydrogels were also reported for management of wounds, yet insufficient adhesion and weak mechanical strength while maintaining moisture can be a concern<sup>6</sup>. Electrospun NFs have demonstrated promising therapeutic benefits such as wound dressings because of their mimicking to the natural extracellular matrix, which facilitate cell adhesion, migration, and tissue regeneration<sup>7</sup>. Additionally, electrospun NFs possess several advantages in wound healing applications due to their high surface area-to-volume ratio and interconnected porosity, and adjustable physicochemical properties<sup>8</sup>. Electrospinning is commonly utilized to fabricate NFs and adjusting electrospinning parameters determines the characteristics of the resultant fibers. Nanofibrous scaffolds can be synthesized using either natural polymers (e.g., collagen, chitosan, and hyaluronic acid), synthetic polymers (e.g., polylactide (PLA), and polyvinyl alcohol (PVA))<sup>9</sup>, or both<sup>10,11</sup>. PVA is a biodegradable synthetic polymer widely used in various applications, including wound dressings, due to its excellent hydrophilicity, biocompatibility, affordability, and crosslinking potential<sup>12,13</sup>. PVA is effective as a wound dressing material *via* maintaining a moist wound environment, enhancing the physical characteristics of the dressing, and accelerating the rate of wound healing<sup>13</sup>. Polylactic acid, also known as polylactide (PLA), is a highly biocompatible and biodegradable synthetic polymer approved by FDA for human use and extensively employed in pharmaceutical and biomedical industries, including tissue engineering, surgical suture fabrication, regenerative medicine, and wound healing<sup>14–17</sup>. PLA-based biomaterials facilitate wound healing by promoting wound area regeneration, collagen formation, angiogenesis, and controlling infection<sup>18</sup>. Incorporation of various natural or synthetic cargoes that possess wound healing properties into nanofibrous scaffolds have demonstrated significant improvement in capacity of tissue healing and regeneration<sup>19</sup>. Roflumilast is a selective phosphodiesterase-4 (PDE4) inhibitor with anti-inflammatory properties<sup>20</sup>. It is indicated for patients with severe chronic obstructive pulmonary disease associated with chronic bronchitis and a history of exacerbations to minimize the risk of further exacerbation. Additionally, it was approved by FDA as a topical cream for plaque psoriasis treatment in July 2022<sup>21,22</sup>. The inhibition of PDE4 leads to elevated intracellular levels of cyclic adenosine monophosphate (cAMP), subsequently reducing pro-inflammatory cytokines such as IL-6, IL-8, and TNF- $\alpha$ , thereby diminishing the recruitment and activation of inflammatory cells<sup>23,24</sup>. Additionally, cAMP controls the migration and proliferation of human keratinocytes by accelerating the re-epithelialization of wounds<sup>25,26</sup>. L-arginine is an endogenous amino acid produced predominantly as a metabolic product of the urea cycle. It is essential for making proteins, urea, creatine, proline, and nitric oxide (NO). The body uses arginine to produce NO, glutamate, and prolamins, which perform various regulatory functions<sup>27,28</sup>. L-arginine has many roles in accelerating wound healing through several biochemical pathways. It promotes blood vasodilation and angiogenesis as a precursor molecule to NO. This increases oxygen and blood delivery to the damaged tissues<sup>29</sup>. L-arginine assists in collagen synthesis by stimulating the production of proline and hydroxyproline, which are essential for extracellular matrix formation and tissue integrity<sup>30</sup>. It also enhances the immune system by stimulating T-cell and macrophage functions and cell proliferation by converting to polyamines *via* the ornithine pathway<sup>31</sup>. Additionally, L-arginine helps the body secrete growth hormone and insulin-like growth factor 1, which are both essential for protein synthesis and tissue growth. This identifies L-arginine an essential amino acid throughout all stages of wound healing<sup>32,33</sup>.

In this study, we developed roflumilast-loaded PLA and L-arginine-loaded PVA nanofibers through a dual-spinneret electrospinning technique. The PLA/PVA blend was chosen to combine the hydrophilicity, swelling capacity, and moisture-retention capabilities of PVA with the advantageous mechanical strength, biodegradability, and prolonged drug release characteristics of PLA, all of which are critical for successful wound healing applications<sup>34</sup>. The two polymers' complementing physicochemical properties allow for the creation of nanofibrous scaffolds that offer tissue regeneration-promoting hydration and structural integrity<sup>35,36</sup>. The aim is to investigate the synergistic effect of these bioactive components on enhancing wound healing rate by combining their diverse pharmacological properties.

## Materials and methods

### Materials

Roflumilast was generously gifted by Al Andalous Pharmaceutical Industries (Egypt). Polylactic acid (PLA) (Ingeo™ 6202D) was purchased from NatureWorks LLC (USA), while L-arginine and chloroform were purchased from Merck (Germany). Polyvinyl alcohol (PVA) was obtained from Alpha Chemika (Mumbai, India).

### Methods

#### *Preparation of electrospun nanofibrous scaffolds*

Two separate polymer solutions were used as the base for dual-spinneret electrospinning. The first solution, PLA was dissolved into chloroform at a concentration of 15% (w/v) by gradually adding the precisely weighed polymer to the solvent under room-temperature and magnetic stirring until a homogeneous, clear solution was obtained. For the second solution, PVA was dissolved in distilled water at 10% (w/v) concentration under 60 °C temperature and stirring conditions to ensure complete dissolution. Drug-loaded solutions were then prepared by adding the active compounds to the polymer matrices through the following procedures: roflumilast powder was added to the PLA solution at 0.5% (w/v) and stirred to become homogeneously dispersed. L-arginine powder was added to the PVA solution at 0.5% (w/v) and was blended until fully dissolved. Roflumilast was added to the PLA solution because it dissolves effectively in chloroform, while L-arginine was incorporated into the PVA solution due to its water solubility. This approach allows us to achieve high solubility for both

Code	Composition	PLA (% w/v)	PVA (% w/v)	Roflumilast (% w/v)	L-arginine (% w/v)	Voltage (kV)
F1	PLA/PVA	15	10	-	-	26.5
F2	PLA-Roflumilast/PVA	15	10	0.5	-	28.5
F3	PLA/PVA-L-arginine	15	10	-	0.5	28.5
F4	PLA-Roflumilast/PVA-L-arginine	15	10	0.5	0.5	28.5

**Table 1.** Composition and concentrations of the components of the nanofibrous scaffolds.

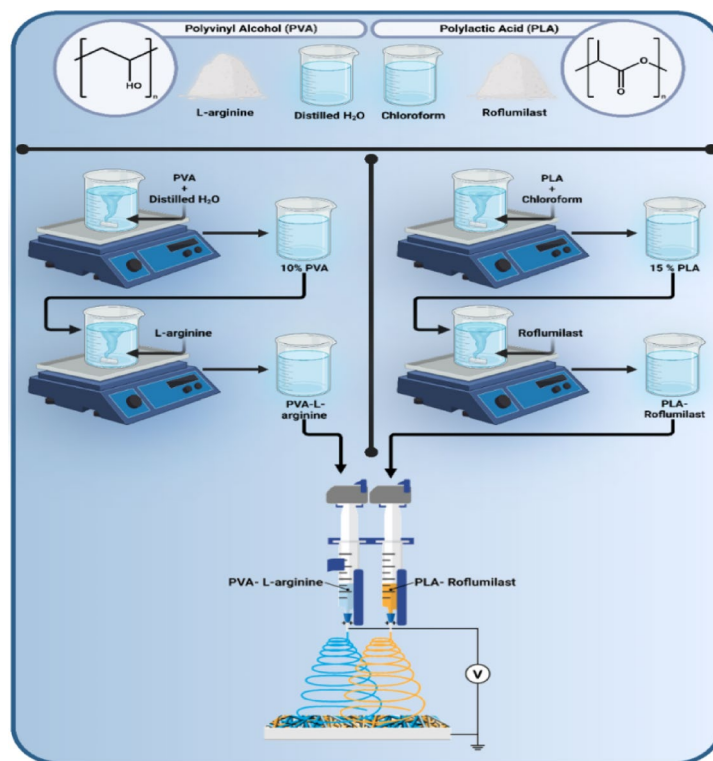


**Fig. 1.** Procedures for fabrication of nanofibrous scaffolds.

substances. The selected concentration was based on previously published studies that show effective and safe loading of L-arginine<sup>31</sup> and roflumilast in topical and electrospun delivery systems<sup>37</sup>. These pilot studies revealed that at concentrations about 0.5% (w/v), maintain the solution spinnability, fiber uniformity, and scaffold integrity, and suboptimal in vivo wound healing performance. Four nanofibrous scaffolds were prepared as follows and their composition and concentrations are demonstrated in Table 1. F1: (PLA/PVA), drug-free control formulation; both spinnerets contained pure polymer solutions, PLA solution and PVA solution. F2: (PLA-Roflumilast/PVA), 0.5% (w/v) roflumilast-loaded PLA solution blended with drug-free PVA solution. F3: (PLA/PVA-L-arginine), drug-free PLA solution blended with 0.5% (w/v) L-arginine-loaded PVA solution. F4: (PLA-Roflumilast/PVA-L-arginine), both solutions were drug-loaded, roflumilast in PLA and L-arginine in PVA. These combinations allowed direct comparison of drug-free, single-drug, and dual-drug-loaded scaffolds under the same electrospinning conditions.

#### Electrospinning process

Nanofiber scaffolds were fabricated using a dual-spinneret electrospinning apparatus (NANON-01 A, MECC, Japan) (Fig. 1). Polymer solutions were loaded in a 5 mL syringe with a 22G stainless steel needle and connected to individual syringe pumps to spin simultaneously. Solutions were electrospun onto a flat plate collector wrapped with aluminum foil. Electrospinning parameters, including applied voltage, tip-to-collector distance, and collector width, were also optimized for even fiber deposition (applied feed rate of 0.5 mL/h, spinneret speed of 100 rpm, spinneret width of 150 mm at a distance of 15 cm, and the applied voltage of 26.5–28.5 kV). All the protocols were carried out in a controlled environment (relative humidity:  $41.0 \pm 2.0\%$ ). After electrospinning, the nanofiber matrices were carefully peeled from the collector and transferred to a vacuum chamber overnight to remove all remaining chloroform and water before characterization.

## Characterizations of nanofibers

### Scanning electron microscopy

The surface morphology of the blended NFs was examined using a field emission environmental scanning electron microscope (FE-SEM) (Quattro S, Thermo Scientific, USA) operated at an acceleration voltage of 15 kV. The samples were observed without any additional coating to ensure accurate imaging and analysis. Further image processing was performed using ImageJ software<sup>38</sup>.

### Fourier transform-infrared spectroscopy

The chemical composition and molecular structure of the NFs scaffolds were analyzed using Fourier Transform Infrared (FT-IR) Spectroscopy. Measurements were conducted using an FT-IR spectrometer (Bruker Vertex 70, Germany), covering the spectral range of 4000–400  $\text{cm}^{-1}$  to identify characteristic functional groups and molecular interactions<sup>39</sup>.

### X-ray diffraction analysis

X-ray diffraction (XRD) diffractometer (Malvern PANalytical, England, UK) with Cu K $\alpha$  radiation was used to examine the crystalline structure of the electrospun NFs. The diffraction patterns were recorded as intensity versus  $2\theta$ , with an angular range of 5° to 80°, a step increment of 0.02°, and a scanning time of 0.5 s per step.

### Study of swelling ratio (%)

The swelling ratio of the NFs was determined based on their ability to absorb water. Pre-weighed NFs ( $W_d$ ) were immersed in 20 mL of deionized water at room temperature for 6 h. After incubation, the NFs were reweighed ( $W_e$ ) in their hydrated condition, and the swelling ratio was estimated at specified time intervals using the following equation:

$$\text{Swelling ratio (\%)} = \left( \frac{W_e - W_d}{W_d} \right) \times 100 \quad (1)$$

A volume of solvent of 20 mL was used in order to create sink conditions and facilitate consistent measurements for swelling under standardized in vitro conditions. This volume was used in order to prevent rapid saturation of the medium, thus facilitating comparisons with respect to swelling characteristics among formulations, rather than attempting to match physiological exudate volume in a wound.

### In vivo wound healing assay

The *in vivo* experiments were ethically approved by Badr University in Cairo-Institutional Ethical Committee No. (BUC-IACUC-241020-115). All methods were carried out in accordance with relevant guidelines and regulations. Twenty male *Wistar* rats (230–250 g) were obtained from the animal house at Badr University in Cairo. The rats were housed in separate polycarbonate cages at 26–28 °C, and a 12-h dark cycle with standard water and food.

A wound healing assay was conducted using twenty male *Wistar* rats. All animals were anesthetized with ketamine (90 mg/Kg) injection, then the back was shaved, and a biopsy punch was used to create 1  $\text{cm}^2$  skin wounds on the back of the rats<sup>40</sup>. To avoid individual differences, rats were randomly divided into **Group I**, which received no treatment, and served as a negative control. **Group II** was treated with F1 (PLA/PVA nanofiber) and served as positive control. **Group III** was treated with F2 (PLA-Roflumilast/PVA nanofiber), **Group IV** was treated with F3 (PLA/PVA-L-arginine nanofiber), and **Group V** was treated with F4 (PLA-Roflumilast/PVA-L-arginine nanofiber) ( $n = 4$ ). Wounds in all groups were covered with sterile gauze to avoid infection. Changes in wound area were measured after 3, 7, 10, and 14 days, the wound area that remained exposed was measured, and the percentage of wound healing was calculated using Eq. (2)<sup>11</sup>:

$$\text{Wound healing \%} = \frac{A_i - A_d}{A_i} \times 100 \quad (2)$$

$A_d$  and  $A_i$  are the wound areas on the specified day and day zero, respectively. The rats in the groups were sacrificed on day 14 by anaesthetizing the rats with intramuscular injections of xylazine (15 mg/kg of body weight) and ketamine (60 mg/kg of body weight). To preserve the skin samples for later histological analysis, they were immediately placed in 10% formalin.

### Histopathological assessment

The wound sites in the four groups were biopsied. Specimens fixed in 10% phosphate-buffered formalin and 3–5  $\mu\text{m}$  sections were prepared and stained with hematoxylin and Eosin stain (H&E). The degree of wound healing was assessed by both granulation tissue and fibrosis as follows:

- Residual granulation tissue indicates delayed wound healing.
- Complete fibrosis indicates complete wound healing.

## Results and discussion

### Construction of dual electrospun nanofibrous scaffolds

Multiple nanofiber scaffolds were produced under varying electrospinning conditions to enhance fiber morphology, uniformity, and layer integrity. The F1 scaffold consisted of a 15% (w/v) PLA solution combined with a 10% (w/v) PVA solution, which served as the standard scaffold and exhibited optimal fiber morphology

and consistency, resulting in smooth and uniform nanofibers. The F2 scaffold was developed with PLA-Roflumilast/PVA, functioning as a single drug-loaded scaffold with a Roflumilast loading concentration of 0.5%. In contrast, the F3 scaffold was created by incorporating 0.5% L-Arginine into a 10% PVA solution, resulting in a PLA/PVA-L-Arginine scaffold. The F4 scaffold integrated both fixed concentrations (0.5%) of each Roflumilast and L-Arginine into a single formulation, labeled as PLA-Roflumilast/PVA-L-Arginine. All scaffolds were electrospun onto a flat plate collector, showcasing randomly oriented fibers with consistent thickness and smooth surfaces.

### SEM investigation

The electrospun nanofibrous scaffolds displayed different morphological and structural characteristics, affirming the effect of drug incorporation and polymer composition on fiber architecture. Figure 2A demonstrates that the PLA/PVA blend produced smooth, bead less fibers with a mean diameter of 0.50  $\mu\text{m}$  and pores area 9.04%. This indicates that the selected polymeric system was electro-spinnable and produced nanoscale fibers suitable for biomedical applications such as drug delivery and tissue engineering<sup>36</sup>. Constant jet stability and optimum process conditions are also supported by the homogenous distribution observed in the histogram. Incorporating roflumilast into the PLA/PVA matrix (Fig. 2B) resulted in a notable increase in fiber diameter to 0.61  $\mu\text{m}$  and pores area to 10.8% and a broader distribution compared to the control sample that might be attributed to the change in solutions' charge density, conductivity, and viscosity during drug loading<sup>41</sup>. The absence of bead formation suggests that the electrospinning process was steady enough to accommodate homogeneous encapsulation inside the fibers. Moreover, introducing L-arginine into the PLA/PVA system (Fig. 2C) also affected fiber morphology, having a mean diameter of 0.55  $\mu\text{m}$  and pores area 11.8%. The introduction of L-arginine, a cationic amino acid, may have improved solution conductivity, allowing thinner fiber generation than the roflumilast-loaded fiber matrix<sup>42</sup>. The NFs incorporating both roflumilast and L-arginine had a mean thickness of 0.62  $\mu\text{m}$ , small pores area 4.8% and a moderately broad distribution (Fig. 2D). The synergistic action between the drug and the charged biomolecule would most likely create competing effects on conductivity and viscosity, leading to thicker fibers<sup>42</sup>. Yet, the morphology was bead-free and uniform, demonstrating that the system could tolerate complex co-loading without defects in processing. These findings support the implication that incorporated drugs can contribute to the electrospun fiber properties. In F2, roflumilast loading increased the mean fiber diameter, whereas adding L-arginine (a cationic amino acid) in F3 likely increased solution conductivity, stabilizing the jet and limiting diameter growth. The observed submicron diameters of fibers are particularly suitable for high surface area to volume ratios to enable efficient drug release and biocompatible interaction with biological tissues.

### FTIR analysis

FTIR spectroscopy was utilized to confirm the successful fabrication of PLA/PVA NFs and determine the loading of roflumilast and L-arginine into the electrospun scaffolds. FTIR is a convenient analytical method for identifying functional groups and monitoring possible interactions among polymers and active pharmaceutical ingredients. The pure polymers (PLA and PVA), pure drugs (roflumilast and L-arginine), and the respective nanofiber composites were compared systematically in terms of spectra. PLA had characteristic absorption

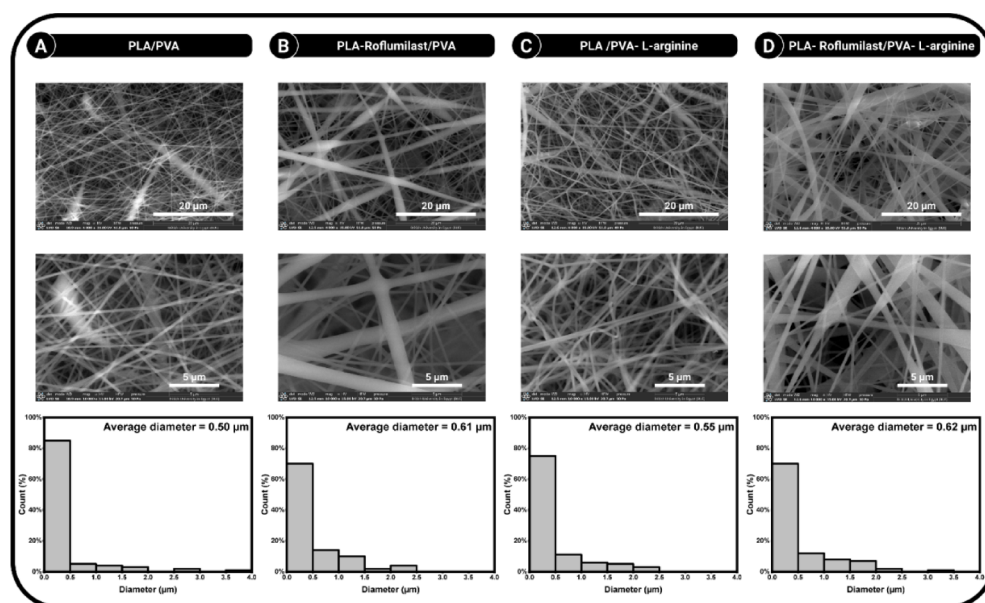


**Fig. 2.** SEM images of (A) (PLA/PVA), (B) (PLA-Roflumilast/PVA), (C) (PLA/PVA-L-arginine), and (D) (PLA-Roflumilast/PVA-L-arginine) NFs. The Lower panel represents diameter distribution histograms of the nanofibers.

bands at  $\nu \sim 1750 \text{ cm}^{-1}$  (ester group C = O stretching),  $\nu \sim 1180\text{--}1085 \text{ cm}^{-1}$  (C–O stretching vibrations), the peaks at  $\nu 755$  and  $867 \text{ cm}^{-1}$  (C–H-bond stretches), and  $\nu \sim 1450\text{--}1380 \text{ cm}^{-1}$  ( $\text{CH}_3$  bending) (Fig. 3A). These peaks reflect the ester backbone and confirm the semi-crystalline nature of PLA<sup>43,44</sup>. PVA exhibited a broad, strong band at  $\nu \sim 3300 \text{ cm}^{-1}$  for O–H stretching typical of hydrogen bonding within the polymer and a shoulder at  $\nu 1142 \text{ cm}^{-1}$  typical of C–O stretching. Peaks at  $\nu 2943 \text{ cm}^{-1}$  and  $2912 \text{ cm}^{-1}$  correspond to the stretching vibrations of the methylene ( $-\text{CH}_2-$ ) and alkyl (C–H) groups, respectively (Fig. 3B). A peak at  $\nu 1712 \text{ cm}^{-1}$  indicates the carbonyl (C = O) stretching vibration, likely from acetate groups. The peaks at  $\nu 1419 \text{ cm}^{-1}$  and  $1375 \text{ cm}^{-1}$  are associated with the bending vibration of the methylene ( $\text{CH}_2$ ) group and the deformation vibration of C–H, respectively. Furthermore, the peak at  $\nu 837 \text{ cm}^{-1}$  is attributed to C–C stretching vibrations. The strong hydrophilic character of PVA is evident in these peaks<sup>45–47</sup>. The spectrum of roflumilast (Fig. 3C) shows several characteristic vibrational peaks that are indicative of its molecular structure. The absorption at  $\nu 3261 \text{ cm}^{-1}$  corresponds to N–H stretching vibrations, while the peaks at  $\nu 3095$  and  $3029 \text{ cm}^{-1}$  are attributed to C–H stretching in the aromatic ring and cyclopropyl group. The aliphatic  $-\text{CH}_2-$  group exhibits symmetric and asymmetric stretching at  $\nu 2921$  and  $2879 \text{ cm}^{-1}$ . A notable peak at  $\nu 1649 \text{ cm}^{-1}$  corresponds to C = O stretching in the amide moiety, and the bands between  $\nu 1594$  and  $1400 \text{ cm}^{-1}$  are associated with C = C stretching in the aromatic ring. Additionally, the peak at  $\nu 1196 \text{ cm}^{-1}$  is due to symmetrical C–O–C stretching within the cyclopropyl group, while the absorption at  $\nu 1155 \text{ cm}^{-1}$  reflects asymmetric stretching of  $-\text{CF}_2-$  group. The peaks at  $869$ ,  $808$ , and  $748 \text{ cm}^{-1}$  indicate C–H out-of-plane bending in the aromatic ring<sup>48,49</sup>. The L-arginine peaks (Fig. 3D) identified at  $\nu 3263 \text{ cm}^{-1}$  and  $3346 \text{ cm}^{-1}$  correspond to the stretching vibrations of the guanidine and primary amine groups, respectively. The peaks at  $\nu 3076 \text{ cm}^{-1}$ ,  $1681 \text{ cm}^{-1}$ ,  $1603 \text{ cm}^{-1}$ , and  $1556 \text{ cm}^{-1}$  are attributed to the stretching vibrations of  $-\text{OH}$  group (from  $-\text{COOH}$ ), C = O, and C = N bonds, alongside the bending vibrations of the N–H bond<sup>50</sup>. PLA/PVA blend spectrum (Fig. 3E) retained the main functional peaks of the two polymers, like the ester C = O stretching of PLA and the broad hydroxyl band of PVA. The overlap of this kind suggested compatibility of the two polymers at the molecular level and the ability to form a stable blended fiber matrix. The broadening of the O–H stretching peak suggested hydrogen bonding interactions between PLA carbonyl groups and PVA hydroxyl groups, potentially leading to enhanced miscibility<sup>36</sup>. The addition of roflumilast into PLA/PVA fibers (Fig. 3F) introduced additional signals to the aromatic moieties and amid functional groups of the drug. Even though these peaks overlapped partly with the polymer background, changes in intensity and minor shifts in carbonyl stretching bands could be observed. These reflect probable hydrogen bonding or dipole–dipole interactions between the functional groups of roflumilast and the polymer chain, maintaining drug dispersion but without any chemical incompatibility<sup>48,49</sup>. Similarly, PLA/PVA fibers with L-arginine (Fig. 3G) showed spectral intensities attributed to the amino acid, specifically in the  $\sim 1650 \text{ cm}^{-1}$  region ( $\text{NH}_2$  bending) and within the broad  $\nu 3200\text{--}3400 \text{ cm}^{-1}$  region. These absorptions blended with the PVA hydroxyl and PLA carbonyl regions are characteristic of hydrogen bonding between L-arginine functional groups and the polymer matrix. This interaction should stabilize drug loading as well as may influence drug release kinetics<sup>50</sup>. In dual-drug loaded formulation (PLA-Roflumilast/PVA-L-arginine) (Fig. 3H), combined features of both bioactive molecules were evident. The presence of both aromatic and amine/carboxylate signals, along with the polymer peaks, confirmed effective co-encapsulation. Interestingly, no new typical peaks were seen, and no substantial shifts indicated chemical degradation or incompatibility. Instead, the broadening of peaks and slight intensity changes in O–H and C = O regions indicate non-covalent physical interactions that hold the composite framework together. Absence of new chemical bonds shows that both roflumilast and L-arginine are

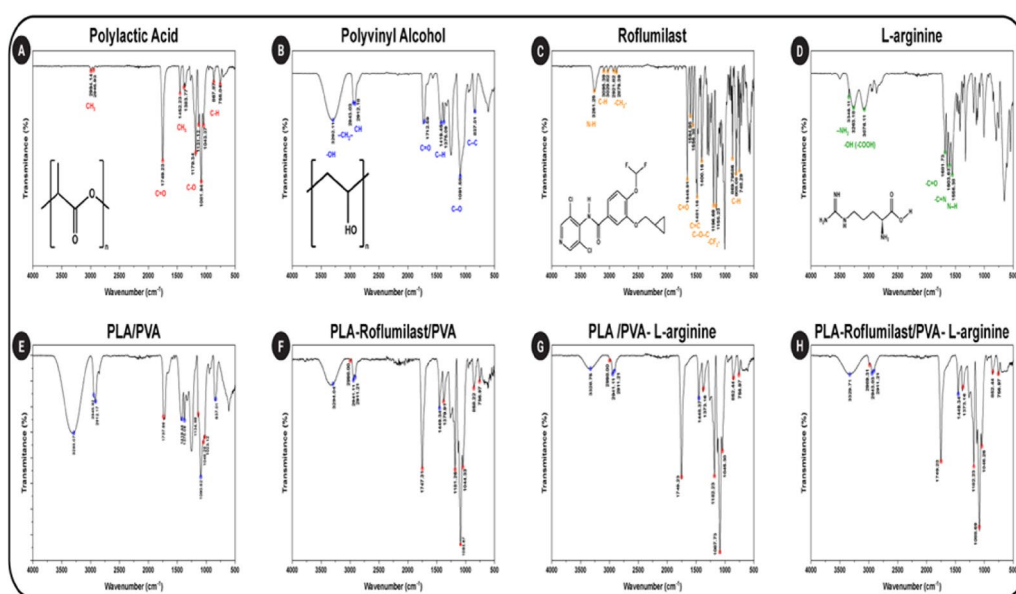


**Fig. 3.** FTIR spectra of (A) PLA, (B) PVA, (C) Roflumilast, (D) L-arginine, (E) (PLA/PVA), (F) (PLA-Roflumilast/PVA), (G) (PLA/PVA-L-arginine), and (H) (PLA-Roflumilast/PVA-L-arginine) NFs.

physically entrapped, rather than chemically conjugated, within the nanofiber matrix. Physical entrapment is advantageous for drug release since it preserves the bioactivity of the loaded drugs and allows controlled release modulated by diffusion and degradation of the polymer<sup>51</sup>. The implied spectral overlaps and hydrogen bonding interactions also indicate a stable drug–polymer network, preventing the risks of the drugs' crystallization or phase separation within the fibers<sup>52</sup>. The FTIR findings confirm that PLA/PVA nanofibers are viable carriers for hydrophobic (roflumilast) as well as hydrophilic (L-arginine) drugs. The drug–polymer compatibility assures fiber structural integrity, whereas the physical interactions found are most likely to ensure drug homogeneity of distribution and reproducible release kinetics.

### XRD analysis

The XRD analysis shows the diffraction patterns of the tested samples, which reflects their structural and phase properties. XRD pattern of roflumilast and L-arginine show a series of sharp and intense diffraction peaks, suggesting a highly crystalline structure (Figs. 4A and B). Roflumilast exhibited typical peaks at  $2\theta = 5.55^\circ, 11.15^\circ, 12.31^\circ, 16.57^\circ, 22.35^\circ, 24.13^\circ,$  and  $48.83^\circ$ , which agree with reported crystalline patterns of the compound<sup>53</sup>. L-arginine exhibited strong peaks at  $2\theta = 9.31^\circ, 11.31^\circ, 15.01^\circ, 16.65^\circ, 19.37^\circ, 23.21^\circ, 27.69^\circ,$  and  $32.01^\circ$ , in accordance with the literature<sup>54,55</sup>. The presence of such typical peaks highlights the good packing architecture of molecules and periodicity in crystalline solids. However, the XRD patterns of the electrospun polymer-based NFs PLA/PVA, PLA-Roflumilast/PVA, PLA/PVA-L-arginine, and PLA-Roflumilast/PVA-L-arginine (Fig. 4C and F) demonstrate a broad amorphous rather than sharp crystalline peaks. This transition to an amorphous pattern indicates that the electrospinning process effectively incorporated roflumilast and L-arginine into the polymer matrix in a non-crystalline form. The transformation of the crystalline drugs into an amorphous state through electrospinning may enhance their dissolution rates and improve bioavailability<sup>56,57</sup>. The ternary formulation with PLA/PVA, roflumilast, and L-arginine (Fig. 4F) did not exhibit crystalline peaks for the drug or amino acid. Instead, the trace showed an amorphous polymeric blend. The complete absence of crystalline peaks indicates that the two active molecules were thoroughly dispersed at the molecular level in the polymeric nanofibers. Amorphous form normally exhibits higher dissolution rates due to greater free energy and a lack of lattice energy barriers. Furthermore, uniform molecular dispersion in the PLA/PVA matrix can prevent recrystallization, giving rise to long-term formulation stability<sup>58</sup>.

### Study of swelling ratio (%)

Swelling properties of the nanofibrous wound dressings also have important clinical applications because they directly correlate to the absorbing capacity of the exudates in the wound and the creation of a moist microenvironment to encourage cell migration, angiogenesis, and re-epithelialization. Excessive swelling could result in the instability of the structure in addition to maceration of the wounds, whilst a low-swelling ratio could cause the adverse effects of poor exudates management<sup>7</sup>. Additionally, the swelling nature of electrospun nanofiber matrices is a critical parameter that controls their drug-releasing ability and hydration stability<sup>59</sup>. The swelling curves of PLA/PVA, PLA-Roflumilast/PVA, PLA/PVA-L-arginine, and PLA-Roflumilast/PVA-L-arginine nanofibers in a period of 6 h at room temperature are illustrated in Fig. 5. The findings exhibit how the

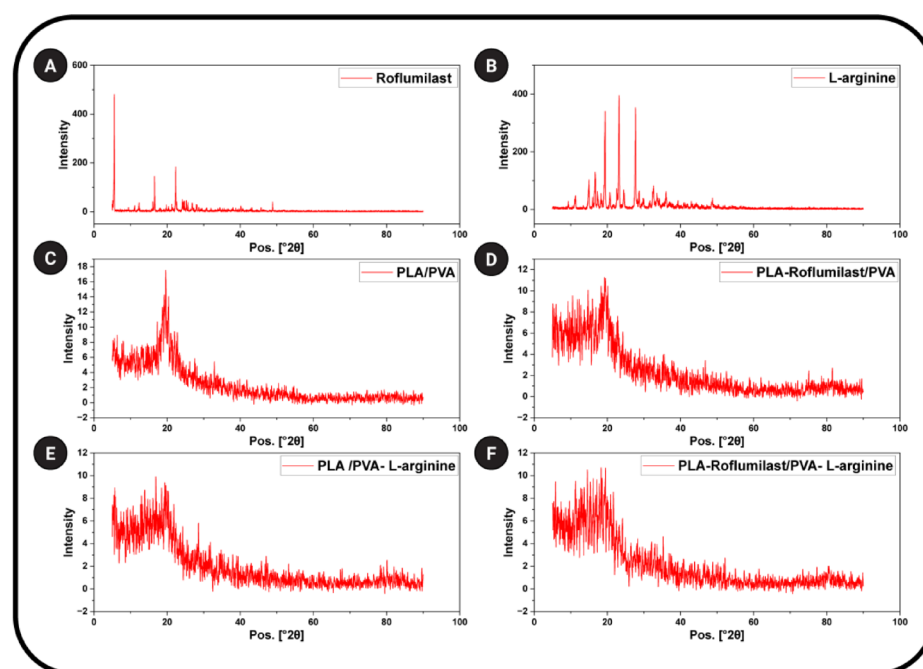


**Fig. 4.** XRD patterns of (A) Roflumilast, (B) L-arginine, (C) (PLA/PVA), (D) (PLA-Roflumilast/PVA), (E) (PLA/PVA-L-arginine), and (F) (PLA-Roflumilast/PVA-L-arginine).

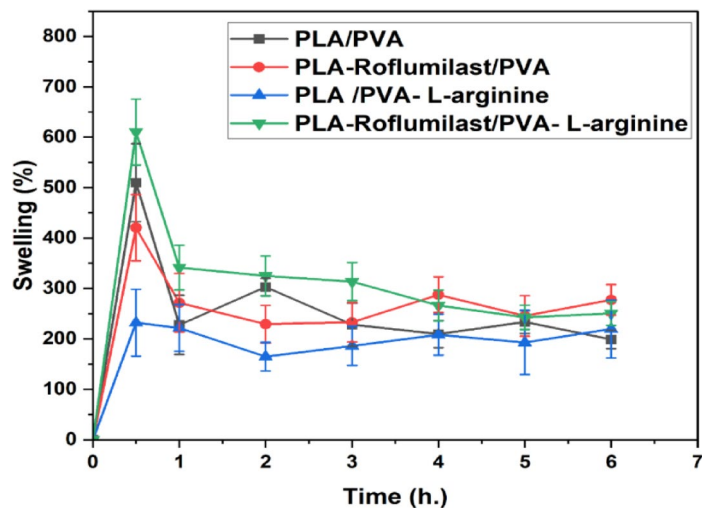


**Fig. 5.** Swelling ratio (%) of the nanofiber scaffolds, PLA/PVA (F1) (Square), PLA-Roflumilast/PVA (F2) (Circle), PLA/PVA-Roflumilast (F3) (Triangle), and PLA-Roflumilast/PVA-Roflumilast (F4) (Inverted triangle).

water-soluble (PVA and L-arginine) and water-insoluble (PLA and Roflumilast) mixtures control the swelling kinetics and stabilization of the nanofibers. The control sample of PLA/PVA exhibited a strongly high initial swelling of ~ 510% during the first hour and slowly reduced to ~ 200%. This is because of the dissolution of PVA to some extent, which is extremely hydrophilic and highly water-absorbent, while the hydrophobic nature of PLA hinders excessive swelling<sup>60,61</sup>. The biphasic appearance observed by initial rapid swelling and stability is common in polymer blends where the amorphous water-soluble phase is accountable for primary hydration and the crystalline or hydrophobic phase is responsible for long-term structural stability<sup>62</sup>.

Roflumilast addition in F2 reduces relative swelling capacity, compared to PLA/PVA (F1) with a maximum swelling of ~ 420% at 1 h, stabilizing to ~ 220%. Roflumilast, being poorly water soluble, would tend to enhance the structural integrity of the NFs to decrease water diffusion channels. As demonstrated in previous research, loading of hydrophobic drug in electrospun fibers inhibited water uptake and altered swelling responses<sup>63</sup>. Moreover, F3 (PLA/PVA-L-arginine) exhibited the lowest swelling overall (~ 220% at 1 h, stabilizing near ~ 190%). Although L-arginine is hydrophilic, its rapid leaching forms drainable pores and its ionic/hydrogen-bond interactions with the polymer phase restrict chain relaxation, thereby reducing bound-water uptake at equilibrium<sup>64</sup>. In contrast, F4 (PLA-Roflumilast/PVA-L-arginine) showed the highest initial swelling (~ 610% at 1 h), driven by the hydrophilicity and osmotic action of the PVA/L-arginine phase, as soluble components dissolved, swelling declined to a moderate plateau (~ 240%), with the hydrophobic PLA/roflumilast framework preserving structural integrity. Thus, L-arginine can promote fast early hydration (F4 spike) while limiting water retention at later times (low plateau), depending on formulation and morphology<sup>65</sup>.

Dissolution of the components over a period caused a reduction in swelling, but the presence of PLA and roflumilast preserved matrix integrity and prevented over-collapsing of the structure. This balance between instant hydration and long-term stability is a desirable character in drug delivery because it allows for initial burst release followed by subsequent duration of sustained release.

Swelling profiles showed that drug loading and polymer composition significantly impact nanofiber hydration and structural stability. As demonstrated by the dual-drug loaded system, excellent swelling capacity can improve the release of amorphous roflumilast to increase bioavailability. Conversely, lower swelling in the L-arginine-loaded system shows controlled release capability with minimal burst effect. These results show that swelling response can be fine-tuned with high specificity to obtain a target drug release profile, with design flexibility for multifunctional therapeutic delivery systems.

### ***In vivo* assessment**

A wound model was developed to assess the wound healing capacity of the developed NFs. The wound images (Fig. 6) were analysed after 3, 7, 10, and 14 days of treatment. The wounds treated with F4 incorporating dual drugs (roflumilast and L-arginine) displayed excellent healing properties as compared to the control untreated group and the group treated with drug-free nanofiber (F1). In the control group, the wound healing rate reached  $24.9 \pm 0.5\%$ ,  $41.2 \pm 0.16\%$ , and  $71.2 \pm 0.1\%$  on the 3rd, 7th, and 10th days (Fig. 7), and large unhealed wounds were identified. The healing rate of wounds treated with F2 (roflumilast-loaded nanofibers), F3 (L-arginine-loaded nanofibers) and F4 (dual-drug loaded nanofibers) ~ 90% on the 10th day of treatment, with almost complete wound closure ( $99.8 \pm 0.5\%$ ) demonstrated in case of group V treated with F4 on day 14, that can be attributed to the presence of roflumilast and L-arginine in the nanofibers. Accordingly, F4 NFs is a potential wound dressing that can expedite wound healing.

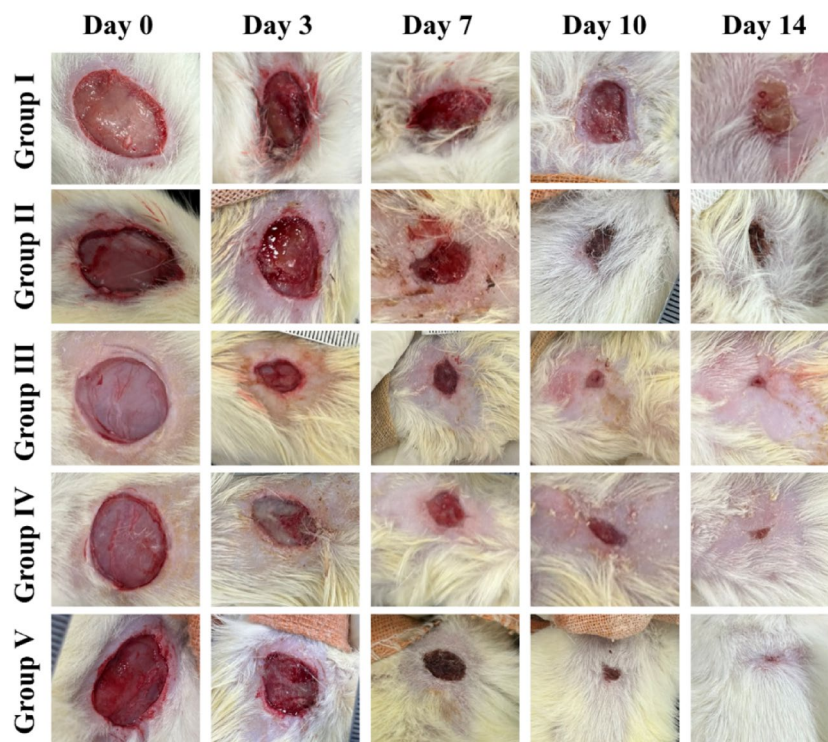


**Fig. 6.** Representative photographic images of wounds for Group I (sterile gauze), Group II (treated with F1), Group III (treated with F2), Group IV (treated with F3), and Group V (treated with F4) on days 0, 3, 7, 10, and 14.

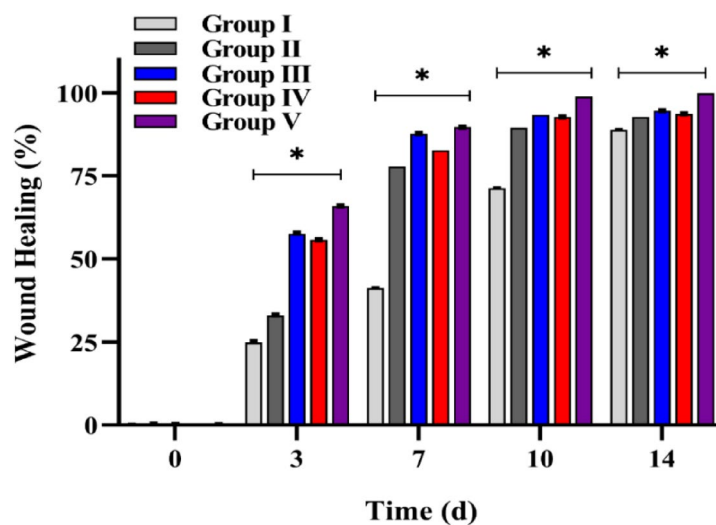


**Fig. 7.** Bar diagram represents the % wound area after treating the wound with drug-loaded nanofibers and the control groups. \* Statistical significance between Group V and Group I ( $p < 0.0001$ ).

### Histopathology study

(Fig. 8A) illustrates a section from the skin wound of Group II revealing residual granulation tissue in the upper dermis and newly formed blood vessels, which indicate delayed wound healing. The covering is intact with complete epithelialization. (Fig. 8B) reveals a section from the skin wound of group III (treated with F2) showing fibrosis in the upper dermis with mild mononuclear inflammatory infiltrate and no residual granulation tissue. The epidermis shows complete epithelial closure. (Fig. 8C) depicts a section from the skin wound of group IV, where residual granulation tissue in the upper dermis and newly formed blood vessels are clearly observed, indicating delayed wound healing. The covering is intact with complete epithelialization. (Fig. 8D) reveals the section from the skin wound of group V showing complete wound healing, as evidenced by the complete fibrosis

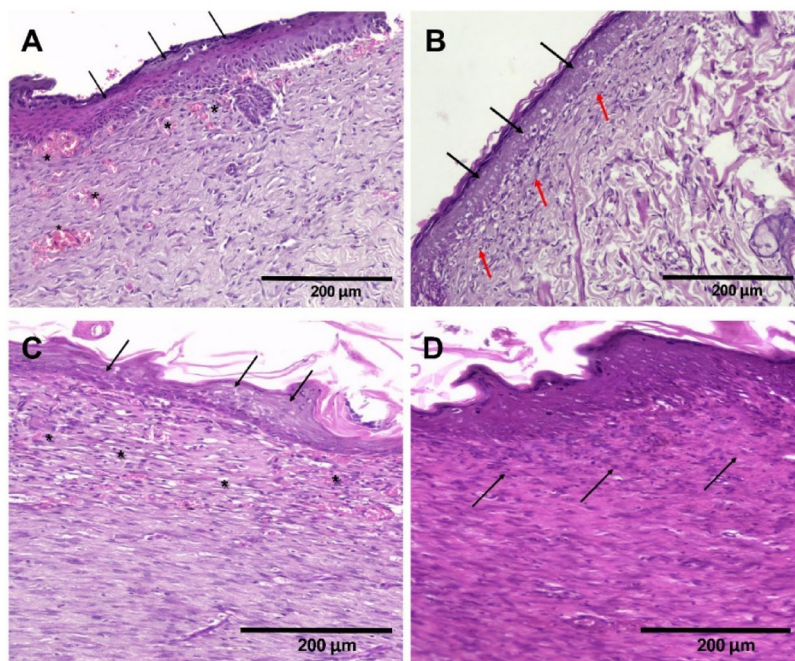


**Fig. 8.** (A) Section from skin wound of group II showing residual granulation tissue in the upper dermis and newly formed blood vessels (\*), indicating delayed wound healing. The covering is intact with complete epithelialization (arrows). H&Ex200 (B) Section from skin wound of group III showing fibrosis in the upper dermis with mild mononuclear inflammatory infiltrate (red arrows) and no residual granulation tissue. The epidermis shows complete epithelial closure (black arrows). H&Ex200 (C) Section from skin wound of group IV showing residual granulation tissue in the upper dermis and newly formed blood vessels (\*), indicating delayed wound healing. The covering is intact with complete epithelialization (arrows). H&Ex200 (D) Section from skin wound of group V shows complete wound healing evidenced by complete fibrosis in the dermis (arrows) with no residual granulation tissue. H&E x200.

in the dermis with no residual granulation tissue. Group II has a similar appearance to Group IV, characterized by residual granulation tissue with minimal fibrosis. In contrast, Group III displays fibrous tissue without any granulation tissue. These results suggest that roflumilast has a more potent effect on wound healing compared to L-arginine. Combined treatment with roflumilast and L-arginine has a more effective response on the wound healing than each component alone, in the form of complete fibrosis with no residual granulation tissue.

## Conclusions

This study successfully demonstrated the development of dual-drug electrospun PLA/PVA NFs loaded with roflumilast and L-arginine as a drug-delivery multifunctional wound dressing system. The morphological and spectroscopical assays confirmed the polymer-drug matrix integrity, and XRD confirmed amorphous dispersion of the two active ingredients, an alteration that enhances dissolution and delays recrystallization. The swelling behavior also demonstrated the capacity of the dual drug loaded scaffold to promote rapid hydration without compromising the long-term structural integrity, a valuable characteristic for controlled drug release. Moreover, biological testing prioritized the therapeutic efficacy of the dual-drug system. *In vivo* studies confirmed the enhanced rate of wound closure, ~99.8% healing on day 14, which was significantly higher compared to single-drug and control groups. Histopathological studies also demonstrated the wound healing properties of the dual drug loaded NFs evidenced by complete fibrosis, absence of granulation tissue, and enhanced re-epithelialization, confirming that the scaffold not only closed the wound but also enabled high-quality tissue formation. Collectively, these findings confirmed the potential delivery of an anti-inflammatory PDE-4 inhibitor and a nitric oxide precursor from a nanofibrous matrix. The system effectively integrates structural, physicochemical, and bioactive functionalities into a single platform with synergistic therapeutic impact. The possibilities extend beyond wound dressings, indicating a broadly applicable drug delivery method with potential for application to the broader fields of tissue engineering and regenerative medicine.

## Data availability

The datasets used and analyzed during the current study are available from the corresponding author on reasonable request.

Received: 5 November 2025; Accepted: 28 January 2026

Published online: 20 February 2026

## References

- Tottoli, E. M. et al. Skin Wound Healing Process and New Emerging Technologies for Skin Wound Care and Regeneration. *Pharmaceutics* **12**, 735. (2020). <https://doi.org/10.3390/PHARMACEUTICS12080735>
- Rousselle, P., Braye, F. & Dayan, G. Re-epithelialization of adult skin wounds: cellular mechanisms and therapeutic strategies. *Adv. Drug Deliv. Rev.* **146**, 344–365. <https://doi.org/10.1016/j.addr.2018.06.019> (2019).
- Rezvani Ghomi, E. et al. Advances in electrospinning of aligned nanofiber scaffolds used for wound dressings. *Curr. Opin. Biomed. Eng.* **22**, 100393. <https://doi.org/10.1016/j.cobme.2022.100393> (2022).
- Mir, M. et al. Synthetic polymeric biomaterials for wound healing: a review. *Prog. Biomater.* **7**, 1. <https://doi.org/10.1007/S40204-018-0083-4> (2018).
- Savencu, I., Iurian, S., Porfire, A., Bogdan, C. & Tomuță, I. Review of advances in polymeric wound dressing films. *React. Funct. Polym.* **168**, 105059. <https://doi.org/10.1016/j.reactfunctpolym.2021.105059> (2021).
- Ho, T. C. et al. Hydrogels: properties and applications in biomedicine. *Molecules* **27**, 2902. <https://doi.org/10.3390/MOLECULES27092902> (2022).
- Jiang, Z. et al. Nanofiber Scaffolds as Drug Delivery Systems Promoting Wound Healing. *Pharmaceutics* **15**, 1829 (2023). <https://doi.org/10.3390/PHARMACEUTICS15071829>
- Eissa, N. G. & Elsbahy, M. Applying drug-loaded electrospun nanofibers to antimicrobial-resistant skin infections. *Nanomedicine* <https://doi.org/10.1080/17435889.2025.2528592> (2025).
- Kamoun, E. A. et al. Recent progress of Polymer-Based biosensors for cancer diagnostic applications: natural versus synthetic polymers. *ACS Omega*. <https://doi.org/10.1021/acsomega.4c10652> (2025).
- Gohar, S. S. et al. Electrospun tamarindus indica-loaded antimicrobial PMMA/cellulose acetate/PEO nanofibrous scaffolds for accelerated wound healing: In-vitro and in-vivo assessments. *Int. J. Biol. Macromol.* **258**, 128793. <https://doi.org/10.1016/j.ijbiomac.2023.128793> (2024).
- Abdelazim, E. B. et al. In vitro and in vivo studies of syzygium cumini-loaded electrospun PLGA/PMMA/collagen nanofibers for accelerating topical wound healing. *RSC Adv.* **14**, 101–117. <https://doi.org/10.1039/D3RA06355K> (2024).
- Vatanpour, V., Teber, O. O., Mehrabi, M. & Koyuncu, I. Polyvinyl alcohol-based separation membranes: a comprehensive review on fabrication techniques, applications and future prospective. *Mater. Today Chem.* **28**, 101381. <https://doi.org/10.1016/j.mtchem.2023.101381> (2023).
- Jin, S. G. Production and application of biomaterials based on Polyvinyl alcohol (PVA) as wound dressing. *Chem. Asian J.* **17**, e202200595. <https://doi.org/10.1002/ASIA.202200595> (2022).
- Maleki, H., Azimi, B., Ismaeilimoghadam, S. & Danti, S. Poly(lactic acid)-Based Electrospun Fibrous Structures for Biomedical Applications. *Appl. Sci.* **12**, 3192 (2022). <https://doi.org/10.3390/APP12063192>
- Pesaranhajiabbas, E., Misra, M. & Mohanty, A. K. Recent progress on biodegradable polylactic acid based blends and their biocomposites: A comprehensive review. *Int. J. Biol. Macromol.* **253**, 126231. <https://doi.org/10.1016/j.ijbiomac.2023.126231> (2023).
- Elsayed, R. E., Madkour, T. M. & Azzam, R. A. Tailored-design of electrospun nanofiber cellulose acetate/poly(lactic acid) dressing Mats loaded with a newly synthesized sulfonamide analog exhibiting superior wound healing. *Int. J. Biol. Macromol.* **164**, 1984–1999. <https://doi.org/10.1016/j.ijbiomac.2020.07.316> (2020).
- Ebrahimi, F., Ramezani, H. & Dana Poly lactic acid (PLA) polymers: from properties to biomedical applications. *Int. J. Polym. Mater. Polym. Biomaterials.* **71**, 1117–1130. <https://doi.org/10.1080/00914037.2021.1944140> (2022).
- Chen, H. L., Chung, J. W. Y., Yan, V. C. M. & Wong, T. K. S. Polylactic Acid-Based biomaterials in wound healing: A systematic review. *Adv. Skin. Wound Care.* **36** <https://doi.org/10.1097/ASW.0000000000000011> (2023).
- Lu, X., Zhou, L. & Song, W. Recent progress of electrospun nanofiber dressing in the promotion of wound healing. *Polym. (Basel)*. **16**, 2596. <https://doi.org/10.3390/POLYM16182596> (2024).
- Christie, P. Roflumilast: a selective phosphodiesterase 4 inhibitor. *Drugs Today (Barc)*. **41**, 667–675. <https://doi.org/10.1358/DOT.2005.41.10.920428> (2005).
- Gyldenløve, M. et al. Efficacy and safety of oral Roflumilast for moderate-to-severe psoriasis—a randomized controlled trial (PSORRO), the lancet regional. *Health - Europe.* **30** <https://doi.org/10.1016/j.lanepe.2023.100639> (2023).
- Wedzicha, J. A., Calverley, P. M. & Rabe, K. F. Roflumilast: A review of its use in the treatment of COPD. *Int. J. COPD.* **11**, 81–90. <https://doi.org/10.2147/COPD.S89849> (2016).
- Zhang, X. et al. Pharmacological mechanism of Roflumilast in the treatment of asthma–COPD overlap. *Drug Des. Devel Ther.* **12**, 2371. <https://doi.org/10.2147/DDDT.S165161> (2018).
- Zhong, B. et al. Roflumilast reduced the IL-18-Induced inflammatory response in Fibroblast-Like synoviocytes (FLS). *ACS Omega.* **6**, 2149. <https://doi.org/10.1021/ACSOMEGA.0C05281> (2021).
- Balakrishnan, B., Mohanty, M., Fernandez, A. C., Mohanan, P. V. & Jayakrishnan, A. Evaluation of the effect of incorporation of Dibutylryl Cyclic adenosine monophosphate in an in situ-forming hydrogel wound dressing based on oxidized alginate and gelatin. *Biomaterials* **27**, 1355–1361. <https://doi.org/10.1016/j.biomaterials.2005.08.021> (2006).
- Ahmed, M. M. et al. Development of Apremilast Nanoemulsion-Loaded Chitosan Gels: In Vitro Evaluations and Anti-Inflammatory and Wound Healing Studies on a Rat Model. *Gels.* **8**, 253 (2022). <https://doi.org/10.3390/GELS8050253>
- Dioguardi, F. S., Corsetti, G., Szlas, A., Kurek, J. M. & Krejpcio, Z. The potential of L-Arginine in prevention and treatment of disturbed carbohydrate and lipid Metabolism—A. *Rev. Nutrients* **2022**, **14**, 961. <https://doi.org/10.3390/NU14050961> (2022).
- Morris, S. M. Arginine: beyond protein. *Am. J. Clin. Nutr.* **83**, 508S–512. <https://doi.org/10.1093/AJCN/83.2.508S> (2006). S.
- Oyovwi, M. O. & Atere, A. D. Exploring the medicinal significance of L-Arginine mediated nitric oxide in preventing health disorders. *Eur. J. Med. Chem. Rep.* **12**, 100175. <https://doi.org/10.1016/j.ejmcr.2024.100175> (2024).
- McKay, T. B., Priyadarsini, S., Rowsey, T. & Karamichos, D. Arginine supplementation promotes extracellular matrix and metabolic changes in keratoconus. *Cells* **10**, 2076. <https://doi.org/10.3390/CELLS10082076/S1> (2021).
- Hussein, Y. et al. Electrospun PVA/hyaluronic acid/L-arginine nanofibers for wound healing applications: nanofibers optimization and in vitro bioevaluation. *Int. J. Biol. Macromol.* **164**, 667–676. <https://doi.org/10.1016/j.ijbiomac.2020.07.126> (2020).
- Wu, M. et al. Recent advances in the development of nitric oxide-releasing biomaterials and their application potentials in chronic wound healing. *J. Mater. Chem. B.* **9**, 7063–7075. <https://doi.org/10.1039/D1TB00847A> (2021).
- Wu, G., Meininger, C. J., McNeal, C. J., Bazer, F. W. & Rhoads, J. M. Role of L-Arginine in nitric oxide synthesis and health in humans. In *Amino Acids in Nutrition and Health: Amino Acids in Gene Expression, Metabolic Regulation, and Exercising Performance* (ed. Wu, G.) 167–187 (Springer International Publishing, 2021). [https://doi.org/10.1007/978-3-030-74180-8\\_10](https://doi.org/10.1007/978-3-030-74180-8_10).
- Elbadry, A. M. M., Gomaa, E., Faisal, M. M., Kamoun, E. A. & Salim, S. A. Smart dressings accelerating wound healing with Tranexamic acid-infused aligned electrospun nanofibers: in vitro and in vivo assessments. *J. Drug Deliv Sci. Technol.* **114**, 107542. <https://doi.org/10.1016/j.jddst.2025.107542> (2025).
- Fatahian, R. & Erfani, R. Surrogate modeling of electrospun PVA/PLA nanofibers using artificial neural network for biomedical applications. *Sci. Rep.* **15**, 12886 (2025). <https://doi.org/10.1038/s41598-025-94608-8>
- Zhong, G. et al. Fabrication and characterization of PVA@PLA electrospinning nanofibers embedded with Bletilla striata polysaccharide and Rosmarinic acid to promote wound healing. *Int. J. Biol. Macromol.* **234**, 123693. <https://doi.org/10.1016/j.ijbiomac.2023.123693> (2023).
- Brown, W. M. Treating COPD with PDE 4 inhibitors. *Int. J. Chron. Obstruct Pulmon Dis.* **2**, 517 (2007). <https://pubmed.ncbi.nlm.nih.gov/articles/PMC2699952/> accessed December 22, 2025.

38. Ashraf, H., Salim, S. A., EL-Moslami, S. H., Loutfy, S. A. & Kamoun, E. A. An injectable in situ forming Collagen/Alginate/CaSO<sub>4</sub> composite hydrogel for tissue engineering applications: Optimization, characterization and in vitro assessments. *Arab. J. Sci. Eng.* <https://doi.org/10.1007/s13369-024-08922-w> (2024).
39. Ibrahim, R. M. et al. Cutting-edge biomaterials for advanced biomedical uses: self-gelation of l-arginine-loaded chitosan/PVA/vanillin hydrogel for accelerating topical wound healing and skin regeneration. *RSC Adv.* **14**, 31126–31142. <https://doi.org/10.1039/d4ra04430d> (2024).
40. Mirmajidi, T., Chogan, F., Rezayan, A. H. & Sharifi, A. M. In vitro and in vivo evaluation of a nanofiber wound dressing loaded with melatonin. *Int. J. Pharm.* **596**, 120213. <https://doi.org/10.1016/j.ijpharm.2021.120213> (2021).
41. Higashi, S., Hirai, T., Matsubara, M., Yoshida, H. & Beniya, A. Dynamic viscosity recovery of electrospinning solution for stabilizing elongated ultrafine polymer nanofiber by TEMPO-CNF. *Sci. Rep.* **10**, 1–8. <https://doi.org/10.1038/S41598-020-69136-2>;SUBJMET A (2020).
42. Xue, J., Wu, T., Dai, Y. & Xia, Y. Electrospinning and electrospun nanofibers: Methods, Materials, and applications. *Chem. Rev.* **119**, 5298. <https://doi.org/10.1021/ACS.CHEMREV.8B00593> (2019).
43. Nguyen, T. T. T., Ghosh, C., Hwang, S. G., Tran, L. D. & Park, J. S. Characteristics of curcumin-loaded Poly (lactic acid) nanofibers for wound healing. *J. Mater. Sci.* **48**, 7125–7133. <https://doi.org/10.1007/S10853-013-7527-Y>;FIGURES/8 (2013).
44. Liu, Y., Liang, X., Wang, S., Qin, W. & Zhang, Q. Electrospun Antimicrobial Poly(lactic acid)/Tea Polyphenol Nanofibers for Food-Packaging Applications. *Polymers* **10**, 561 (2018). <https://doi.org/10.3390/POLYM10050561>
45. Hashmi, M., Ullah, S. & Kim, I. S. Electrospun momordica Charantia incorporated Polyvinyl alcohol (PVA) nanofibers for antibacterial applications. *Mater. Today Commun.* **24**, 101161. <https://doi.org/10.1016/J.MTCOMM.2020.101161> (2020).
46. Ge, J. C., Wu, G., Yoon, S. K., Kim, M. S. & Choi, N. J. Study on the Preparation and Lipophilic Properties of Polyvinyl Alcohol (PVA) Nanofiber Membranes via Green Electrospinning. *Nanomaterials* **11**, 2514 (2021). <https://doi.org/10.3390/NANO11102514>
47. Abd El-aziz, A. M., El-Maghraby, A. & Taha, N. A. Comparison between Polyvinyl alcohol (PVA) nanofiber and Polyvinyl alcohol (PVA) nanofiber/hydroxyapatite (HA) for removal of Zn<sup>2+</sup> ions from wastewater. *Arab. J. Chem.* **10**, 1052–1060. <https://doi.org/10.1016/J.ARABJC.2016.09.025> (2017).
48. Maded, Z. K. et al. Development and optimization of Dipyridamole- and Roflumilast-Loaded nanoemulsion and nanoemulgel for enhanced skin permeation: Formulation, Characterization, and in vitro assessment. *Pharmaceuticals* **17**, 803. <https://doi.org/10.3390/PH17060803/S1> (2024).
49. Ali, F., Kumar, R., Sahu, P. L. & Singh, G. N. Physicochemical characterization and compatibility study of Roflumilast with various pharmaceutical excipients. *J. Therm. Anal. Calorim.* **130**, 1627–1641. <https://doi.org/10.1007/S10973-017-6274-8>;TABLES/4 (2017).
50. Lv, J. et al. Deep eutectic solvents based on L-Arginine and 2-Hydroxypropyl-β-Cyclodextrin for drug carrier and penetration enhancement. *AAPS PharmSciTech.* **24**, 1–12. <https://doi.org/10.1208/S12249-023-02638-0>;TABLES/3 (2023).
51. Mohammadian, F. & Eatemadi, A. Drug loading and delivery using nanofibers scaffolds. *Artif. Cells Nanomed. Biotechnol.* **45**, 881–888. <https://doi.org/10.1080/21691401.2016.1185726> (2017).
52. Elbadry, A. M. M. et al. Enhancing topical delivery of N-acetylcysteine and collagen via a novel electrospun collagen/PMMA nanofibrous Mats as facial mask development: nanofibers optimization and in vitro experiments. *J. Drug Deliv Sci. Technol.* **104** <https://doi.org/10.1016/j.jddst.2024.106566> (2025).
53. Roflumilast crystal form compound, preparation method, composition and applications thereof. (2011).
54. Mahmoud, A. A., Elkasaby, N. A. & Abdelkhalik, A. A. Design and characterization of emulsified spray dried alginate microparticles as a carrier for the dually acting drug Roflumilast. *Eur. J. Pharm. Sci.* **122**, 64–76. <https://doi.org/10.1016/J.EJPS.2018.06.015> (2018).
55. Mallik, T. & Kar, T. Growth and characterization of nonlinear optical l-arginine dihydrate single crystals. *J. Cryst. Growth.* **285**, 178–182. <https://doi.org/10.1016/J.JCRYSGRO.2005.08.025> (2005).
56. Yu, D. G., Li, J. J., Williams, G. R. & Zhao, M. Electrospun amorphous solid dispersions of poorly water-soluble drugs: A review. *J. Controlled Release.* **292**, 91–110. <https://doi.org/10.1016/J.JCONREL.2018.08.016> (2018).
57. Huo, P. et al. Electrospun Nanofibers of Polycaprolactone/Collagen as a Sustained-Release Drug Delivery System for Artemisinin. *Pharmaceutics* **13**(13), 1228. <https://doi.org/10.3390/PHARMACEUTICS13081228> (2021).
58. de Mohac, L. M., Keating, A. V., de F. Pina, M. & Raimi-Abraham, B. T. Engineering of nanofibrous amorphous and crystalline solid dispersions for oral drug delivery. *Pharmaceutics* **11**, 7. <https://doi.org/10.3390/PHARMACEUTICS11010007> (2018).
59. Mirzaeei, S., Taghe, S., Asare-Addo, K. & Nokhodchi, A. Polyvinyl Alcohol/Chitosan Single-Layered and Polyvinyl Alcohol/Chitosan/Eudragit RL100 Multi-layered electrospun nanofibers as an ocular matrix for the controlled release of ofloxacin: an in vitro and. *Vivo Evaluation AAPS PharmSciTech.* **22**, 1–13. <https://doi.org/10.1208/S12249-021-02051-5>;TABLES/2 (2021).
60. Çay, A. & Mirafteb, M. Perrin Akçakoca Kumbasar, characterization and swelling performance of physically stabilized electrospun poly(vinyl alcohol)/chitosan nanofibres. *Eur. Polym. J.* **61**, 253–262. <https://doi.org/10.1016/J.EURPOLYMJ.2014.10.017> (2014).
61. Karami, Z., Rezaeian, I., Zahedi, P. & Abdollahi, M. Preparation and performance evaluations of electrospun poly(ε-caprolactone), poly(lactic acid), and their hybrid (50/50) nanofibrous Mats containing thymol as an herbal drug for effective wound healing. *J. Appl. Polym. Sci.* **129**, 756–766. <https://doi.org/10.1002/APP.38683> (2013).
62. Protsak, I. S. & Morozov, Y. M. Fundamentals and Advances in Stimuli-Responsive Hydrogels and Their Applications: A Review. *Gels*, **11**, 30 (2025). <https://doi.org/10.3390/GELS11010030>
63. Sill, T. J. & von Recum, H. A. Electrospinning: applications in drug delivery and tissue engineering. *Biomaterials* **29**, 1989–2006. <https://doi.org/10.1016/J.BIOMATERIALS.2008.01.011> (2008).
64. Annabi, N. et al. Controlling the porosity and microarchitecture of hydrogels for tissue engineering. *Tissue Eng. Part. B Rev.* **16**, 371. <https://doi.org/10.1089/TEN.TEB.2009.0639> (2010).
65. Roy, S. G., Halder, U. & De, P. Remarkable swelling capability of amino acid based cross-linked polymer networks in organic and aqueous medium. *ACS Appl. Mater. Interfaces.* **6**, 4233–4241. <https://doi.org/10.1021/AM405932F>;SUPPL\_FILE/AM405932F\_SI\_001.PDF (2014).

## Author contributions

Samar Salim: Conception, Experiments, Data analysis, Supervision, Revised the final draft; Abdullah Elbadry : Experiments, Data acquisition, Interpretation of data, Wrote the original draft; Esraa B. Abdelazim: *In vivo* study, Wrote original draft and Data analysis, Tasneem Abed: *In vivo* study and Data analysis; Marwa Mosaad Shakweer : Histopathological study; Noura Eissa: Data analysis, Draft revision; E. A. Kamoun : Design of the work, Draft revision, Supervision, Revised the final draft; Mahmoud Elsabahy : Data analysis, Draft revision, Supervision.

## Funding

Open access funding provided by The Science, Technology & Innovation Funding Authority (STDF) in cooperation with The Egyptian Knowledge Bank (EKB).

## Declarations

### Competing interests

The authors declare no competing interests.

### Ethical approval

The in vivo experiments were ethically approved by Badr University in Cairo-Institutional Ethical Committee No. (BUC-IACUC-241020-115). All methods are reported in accordance with ARRIVE guidelines.

### Additional information

**Correspondence** and requests for materials should be addressed to S.A.S., E.A.K. or M.E.

**Reprints and permissions information** is available at [www.nature.com/reprints](http://www.nature.com/reprints).

**Publisher's note** Springer Nature remains neutral with regard to jurisdictional claims in published maps and institutional affiliations.

**Open Access** This article is licensed under a Creative Commons Attribution 4.0 International License, which permits use, sharing, adaptation, distribution and reproduction in any medium or format, as long as you give appropriate credit to the original author(s) and the source, provide a link to the Creative Commons licence, and indicate if changes were made. The images or other third party material in this article are included in the article's Creative Commons licence, unless indicated otherwise in a credit line to the material. If material is not included in the article's Creative Commons licence and your intended use is not permitted by statutory regulation or exceeds the permitted use, you will need to obtain permission directly from the copyright holder. To view a copy of this licence, visit <http://creativecommons.org/licenses/by/4.0/>.

© The Author(s) 2026